Research Square

Preprints are preliminary reports that have not undergone peer review.
They should not be considered conclusive, used to inform clinical practice,
or referenced by the media as validated information.

Remembering like a Brain: A Bio-Inspired Associative Memory Model integrating Hodgkin-Huxley Dynamics and Modular Network Architecture

Diletta Bartolini
University of Pavia
Miranda Bellezza
University of Florence
Azzurra Palma
University of Florence
Andrea Frosini
andrea.frosini@unifi.it
University of Florence
Vincent Pelletier
University of Poitiers

Research Article

Keywords: Associative memory, Hodgkin–Huxley model, Hopfield network, graph theory, computational models, heterogeneous firing patterns, synaptic coupling

Posted Date: November 7th, 2025

DOI: https://doi.org/10.21203/rs.3.rs-7903733/v1

License: This work is licensed under a Creative Commons Attribution 4.0 International License.
Read Full License

Additional Declarations: No competing interests reported.

Remembering like a Brain: A Bio-Inspired Associative Memory Model integrating Hodgkin-Huxley Dynamics and Modular Network Architecture

Diletta Bartolini[1], Miranda Bellezza[2], Azzurra di Palma[2], Andrea Frosini [*2], and Vincent Pelletier [†3]

[1] *Department of Mathematics, University of Pavia, Pavia - Italy, Faculty of Mathematics and Computer Science, UniDistance Suisse, Brig - Switzerland; diletta.bartolini01@universitadipavia.it (D.B.)*
[2] *Department of Mathematics and Informatics, University of Florence, Florence, Italy; miranda.bellezza@unifi.it (M.B.); azzurra.dipalma@unifi.it (A.d.P.); andrea.frosini@unifi.it (A.F.)*
[3] *Unit for Training and Research in Fundamental and Applied Sciences, University of Poitiers, Poitiers - France*

Abstract

Associative memory enables the retrieval of stored information from incomplete or noisy cues and supports cognitive functions such as pattern recognition, decision-making, and learning. Computational models, particularly Hopfield-type networks, have provided valuable insights into the basis of these processes. However, many existing models overlook important biological factors, including realistic neuronal dynamics, synaptic variability, and inhibitory mechanisms, which limits their neurobiological plausibility.

Building upon the model by H. Hasegawa (2001), we propose a novel associative memory model that integrates biologically realistic Hodgkin-Huxley-type neurons within a modular Hopfield network architecture. Our model incorporates the three predominant neuron types found in the mammalian brain, facilitating the simulation of complex network interactions such as lateral inhibition and disinhibition. This biologically inspired framework supports both chemical and electrical synapses, dynamic connectivity, and a modular network structure, thereby enhancing the biological realism and computational efficiency of memory process modeling.

Our network consists of a three layered architecture of N extended spiking Hodgkin-Huxley neurons with time-delayed couplings that store P patterns through their synaptic weights.

Our simulations show high network performances with an accurate biological fidelity, achieving a storage capacity ($\alpha_c = P_{max}/N \sim 0.7$) for low neuron activity ($f = 0.1$), which represents a significant improvement compared to previous associative memory models.

Keywords: Associative memory, Hodgkin–Huxley model, Hopfield network, graph theory, computational models, heterogeneous firing patterns, synaptic coupling.

[*]Corresponding author.
[†]Authors are listed in alphabetical order.

1 Introduction

Associative memory is one of the fundamental functions of neural systems, allowing the recall of stored information from noisy or partial input [1]. This mechanism is essential for most cognitive tasks, such as pattern recognition, decision-making and learning [2]. In computational neuroscience, associative memory models have been developed to replicate this capability and to gain insight into how brain stores, encodes, and retrieves information. Among these, Hopfield-type neural networks have been extensively examined as simplified models of learning and memory processes in the brain [3]. Such networks are typically fully connected and symmetric, with information stored in the connection weights according to a Hebbian learning rule. The stored patterns act as fixed-point attractors in the network dynamics, allowing memory retrieval by the system settling into one of these configurations. Despite their theoretical usefulness, Hopfield networks remain highly abstract and differ significantly from biological neural circuits. In particular, they clarify several limitations in terms of biological plausibility, including:

1. *Rate coding vs. temporal coding.* Hopfield networks rely on rate-based representations, whereas increasing experimental evidence highlights the importance of precise spike timing (temporal coding) in memory processes [4, 5, 6].

2. *Simplified synaptic mechanisms.* The original Hopfield model assumes symmetric connections and static synaptic rules, which do not reflect the complex and dynamic nature of synaptic behavior observed in biological networks [7].

3. *Absence of inhibitory dynamics.* Biological systems rely heavily on inhibitory interactions, such as lateral inhibition, which are absent in classic Hopfield networks. These mechanisms contribute to noise reduction, pattern discrimination, and robust memory recall [8, 9].

4. *Biophysical oversimplifications.* Neurons in Hopfield networks are modeled as binary units, ignoring the rich ionic and dynamical properties of real neurons, which exhibit complex behaviors like action potential generation, ion channel dynamics, and intracellular signaling [7].

5. *Non-biological connectivity.* Real neural networks are sparsely connected, whereas Hopfield networks are fully connected [10, 11].

Recent researches started to address these limitations. For example, Hideo Hasegawa ([12]) proposed a biologically realistic associative memory model based on the temporal coding of Hodgkin-Huxley neurons, a detailed biophysical model of neuronal activity originally developed in 1952 [13, 14]. Unlike classic Hopfield networks, this model employs spike timing and binary synapses trained with the Willshaw rule [15], a refinement of the Hebbian learning rule. It demonstrates robust memory capacity and noise resilience, partly due to the inclusion of inhibitory mechanisms that reduce interference during retrieval. Despite these strengths, the model also has limitations, which we discuss in detail in Section 2.5.
Hasegawa's model serves as a foundation for subsequent efforts to model and study associative memory networks, and it constitutes a valuable benchmark for our study.
Other approaches exist as well. For instance, [16] incorporates reinforcement learning into a small Hopfield network, partially addressing some biological challenges but remains limited in scale and performance. Similarly, [17] introduces spiking behavior but struggles with scalability due to computational overhead.

A notable feature of the model in [12] is that neurons of the same type have connections mimicking both excitatory and inhibitory synapses. Although excitatory connections are strengthened when neurons share stored patterns, inhibition is implemented as a uniform static mechanism applied equally throughout the network, primarily to suppress excessive activity. Moreover, the model assumes full connectivity, which is unrealistic biologically since real neural circuits are typically sparse and modular.

To address these points, our model proposes a more biologically inspired associative memory framework building on the pioneering work in [18]. It integrates different types of neurons that interact within a structured Hopfield-like architecture, enabling efficient and realistic pattern storage and retrieval to enhance memory recall capacity. In this work, we propose an associative memory model that bridges the gap between abstract Hopfield networks and biologically realistic neural dynamics, while maintaining computational efficiency. Our goal is to overcome several key issues still present in recent associative models based on [12]. We briefly outline these challenges below and provide further details in *Section* 4.

Specifically, we include the three most common neuron types found in the mammalian brain [19], each characterized by distinct firing pattern: Fast-Spiking (FS), Regular-Spiking with Adaptation (RSA), and Intrinsic Bursting (IB). These neurons are interconnected through both chemical and electrical synapses, modeled with separate differential equations to accurately capture the dual nature of synaptic transmission.

A key innovation is the implementation of inhibitory mechanisms that go beyond the uniform inhibition of [12], introducing biologically inspired lateral inhibition and disinhibition.

FS neurons act as inhibitory units with synaptic weights governed by the inverse of the Willshaw rule. These inhibitory circuits are organized modularity to slow activation in a specific network area that mimics biological cortical networks [20].

On the one hand, lateral inhibition is well documented, on the other hand, it has rarely been incorporated into Hopfield-type memory systems. One attempt is found in [21], where a simple feedforward lateral inhibition network replicates basic visual functions such as edge detection and contrast enhancement.

Disinhibition, which occurs through FS-FS neuron interactions, allows transient suppression of inhibitory activity itself, refining temporal control over neural dynamics.

We successfully model disinhibition by adding a third modulation layer regulating FS neurons via inhibitory pathways. This "inhibition of inhibition" produces a net excitatory effect on principal neurons without directly modulating their inputs, thus breaking the excitation-inhibition balance [22].

Another novel aspect is the feedback architecture inspired by graph theory, which separates individual neuronal dynamics from collective network behavior. This design enables scalable simulations, and clearer analysis of emergent phenomena.

Our approach overcomes common challenges in associative memory models, reproducing learning and memory behaviors consistent with experimental observations while remaining computationally tractable.

Finally, separating neuronal parameters from connectivity matrices allows independent manipulation of components, facilitating studies of large-scale networks and emergent phenomena such as synchronization, plasticity, and memory consolidation.

The paper is organized as follows:

- *Section* 2 introduces the Hodgkin-Huxley neuronal model and its biophysical features, followed by the Hopfield network and Hasegawa's model of associative memory, which serves as a benchmark;

- *Section* 3 sheds light on our proposed memory model from a topological perspective, including parameter settings and retrieval functions;
- *Section* 4, we analyze the storage and retrieval capabilities of our network, with particular focus on perfect input presentations. Here, we define the maximum storage capacity and compare the performance of our model with that of the Hasegawa's model, highlighting their differences and similarities;
- Finally, *Section* 5 provides concluding remarks, summarizing the key findings and discussing potential future extensions, including the integration of learning mechanisms for dynamic weight adaptation.

2 Methods

Here, we provide a detailed description of the main neuronal activity models considered in our study. For each model, we present the governing equations to ensure full understanding and reproducibility. Moreover, we describe the Hopfield network, which forms the foundational framework for associative memory storage and retrieval.

Extended Hodgkin-Huxley Model

Much of our knowledge in the field of synaptic transmission mechanisms originates from the pioneering studies of A.L. Hodgkin and A.F. Huxley on the giant squid axon. Their pioneering experiments in the early 1950s yielded essential insights into the propagation of electrical signals in neurons, providing a cornerstone for the field of modern neuroscience. Their model, briefly indicated as the HH model, first presented in [13], consists of a non-linear dynamical system that describes how ion-specific channels (or gates) regulate ion flow across the neuronal membrane, forming the foundation for the generation of action potentials. These ion channels open when ionic currents across the membrane reach a threshold sufficient to activate them, causing a rapid change in membrane potential due to fluctuations in electrical potential and ion concentration.
The permeability of the membrane to ions, as observed for sodium (Na^+) and potassium (K^+), varies abruptly during depolarization to restore the membrane to its resting potential. The membrane potential governs the rates and equilibrium values of the activation and inactivation mechanisms that control these permeability changes. However, the generation of an action potential is not simply a passive fluctuation of membrane potential but follows a well-defined sequence of events. In the rest, when the neuron is not stimulated, the interior of the cell membrane is negatively charged relative to the exterior. It typically ranges between -60 mV and -70 mV. This resting potential is maintained by the differential distribution of ions across the membrane and the selective permeability of ion channels, primarily through the movement of Na^+ and K^+ ions.
When the membrane potential depolarizes by approximately 15 mV from its resting state, it reaches a critical threshold at which the neuron fires, initiating an action potential. This firing event is predominantly driven by the rapid influx of Na^+ ions entering the neuron through voltage-gated sodium channels, causing a sharp rise on membrane potential. Following this peak, the neuron begins to polarize again. This process is mediated by two distinct mechanisms: potassium channels open, allowing K^+ ions to exit the neuron and restore the negative internal charge, while sodium channels become inactivated, preventing further Na^+ influx. The membrane potential continues to hyperpolarize gradually as potassium flows outward, dropping below the resting potential before

stabilizing. This period (called refractory period) ensures that the neuron does not fire immediately again, allowing unidirectional propagation of the action potential along the axon.
Real biological neurons exhibit a wide range of firing patterns, shaped by their structural and functional characteristics. While the HH model provides a foundational explanation of action potential generation, it captures only a limited aspect of neuronal behavior. To more accurately reflect the diversity of real neuronal responses, the model must be extended to include additional ionic currents that regulate excitability and adaptation. The original HH model accounted only for neurons firing at regular intervals, thus producing a stereotypical regular spiking pattern, in contrast, neurons in the human brain display a much broader variety of firing behaviors, modulating their activity depending on their location, function, and the nature of external inputs (see [23]).
In literature, three main classes of neurons have been identified in neural dynamics, as reported in [24], they are:

1) *Fast Spiking neurons*, known for rapid and consistent firing with minimal adaptation, critical for the processing of sensory information [25]. These kinds of neurons provide fast inhibition that synchronizes neuronal activity and is critical to cognitive function in the cortex [26].

2) *Regular Spiking with Adaptation neurons*, characterized by an initial burst of high-frequency spikes, followed by firing at a lower, constant rate [27]. If a neuron is stimulated repeatedly and for a prolonged time, for example, by constant sensory stimulation or artificially by applying an electric current, it first shows a strong onset response, followed by an increase in the time between spikes [28].

3) *Intrinsic Bursting neurons*, these neurons produce bursts of action potentials followed by quiescent periods, essential for motor and sensory functions [19].

Therefore, the membrane potential $V(t)$ can be described by a differential equation in which Na^+ and K^+ play a central role. To extend the HH model and consider these different firing patterns, Pospischil [29] introduces modifications to the HH potential equation, specifically adding significant currents of calcium channels, i.e., g_{Ca} and E_{Ca} for RSA neurons, and slow sodium g_M channels for IB neurons. For each neuron, the general updated formula for the membrane potential $V(t)$ evolution is expressed as:

$$\begin{aligned}\frac{\delta V(t)}{\delta t} =& \frac{1}{C}\Big(I_{in}(t) - g_L\big(V(t)-E_L\big) - g_K n^4(t)\big(V(t)-E_K\big) - g_M p(t)\big(V(t)-E_K\big) + \\ &- g_{Na} m^3(t) h(t)\big(V(t)-E_{Na}\big) - g_{Ca} q^2(t) s(t)\big(V(t)-E_{Ca}\big)\Big)\end{aligned} \tag{1}$$

Where:
- C is the membrane capacity;
- I_{in} is the external current applied to the neuron;
- g_{Na}, g_K,g_M, g_{Ca}, g_L are voltage-dependent conductance for Na^+, K^+, slow K^+, Ca^+, and leak channel, respectively (*Table* 1);
- E_{Na}, E_K, E_{Ca} and E_L are the reversal potentials for Na^+, K^+, Ca^+, and the leak channel, respectively (*Table* 1).

The gating variables which represent activation and inactivation of ion channels, follow the first-order differential equations:

$$\begin{cases} \frac{dx}{dt} = \alpha_x(1-x) - \beta_x x \\ \\ \frac{\delta p(t)}{\delta t} = \frac{p_\infty(t) - p(t)}{p_\tau(t)} \end{cases} \tag{2}$$

Parameters	**IB**	**RSA**	**FS**	**units**
C	1	1	0.5	$\frac{\mu F}{cm^2}$
E_k	-90	-90	-90	mV
E_{Ca}	120	0	0	mV
E_{Na}	50	56	50	mV
E_L	-70	-70.3	-70	mV
g_K	5	6	10	$\frac{mS}{cm^2}$
g_M	0.03	0.075	0	$\frac{mS}{cm^2}$
g_{Ca}	0.2	0	0	$\frac{mS}{cm^2}$
g_{Na}	50	56	56	$\frac{mS}{cm^2}$
g_L	0.01	2.05×10^{-2}	1.5×10^{-2}	$\frac{mS}{cm^2}$
τ_{max}	608	608	1	$msec$
V_T	-56.2	-56.2	-56.2	mV
V_{syn}	20	20	-80	mV

Table 1: Biophysical parameters used in HH models according to the three types of neurons in the network: IB, RSA and FS. Each column contains the values of parameters used to define the membrane and channel properties of the corresponding class of neurons. Parameters are, respectively, membrane capacitance C, equilibrium potentials E_k, E_{Ca}, E_{Na}, and E_L, maximum conductances for potassium E_K, M-type g_M, calcium g_{Ca}, sodium g_{Na}, and leak g_L channels, synaptic and threshold parameters τ_{max}, V_T, and V_{syn}.

when the variable $x \in \{m(t), n(t), h(t), q(t), s(t)\}$. The parameters involved in *Equations* (2) are reported in *Table* 1, while the remaining equations are defined as follows:

$$\alpha_n(t) = \big(V(t) - V_T - 15\big)\frac{-0.032}{\exp\Big(\frac{-\big(V(t)-V_T-15\big)}{5}\Big) - 1}$$

$$\alpha_m(t) = \big(V(t) - V_T - 13\big)\frac{-0.32}{\exp\Big(\frac{-\big(V(t)-V_T-13\big)}{4}\Big) - 1}$$

$$\alpha_h(t) = 0.128\exp\Big(\frac{-\big(V(t) - V_T - 17\big)}{18}\Big)$$

$$\alpha_q(t) = \big(-27 - V(t)\big)\frac{0.055}{\exp\big(\frac{-27-V(t)}{3.8}\big) - 1}$$

$$\alpha_s(t) = 0.000457\exp\Big(\frac{\big(-13 - V(t)\big)}{50}\Big)$$

$$p_\infty(t) = \frac{1}{\exp\Big(\frac{-\big(V(t)+35\big)}{10}\Big) + 1}$$

$$\beta_n(t) = 0.5\exp\Big(\frac{-\big(V(t) - V_T - 10\big)}{40}\Big),$$

$$\beta_m(t) = \big(V(t) - V_T - 40\big)\frac{0.28}{\exp\big(\frac{V(t)-V_T-40}{5}\big) - 1}$$

$$\beta_h(t) = \frac{4}{\exp\Big(\frac{-\big(V(t)-V_T-40\big)}{5}\Big) + 1}$$

$$\beta_q(t) = 0.94\exp\big(\frac{-75 - V(t)}{17}\big)$$

$$\beta_s(t) = \frac{0.0065}{\exp\big(\frac{-15-V(t)}{28}\big) + 1}$$

$$p_\tau(t) = \frac{\tau_{max}}{3.3\exp\Big(\frac{V(t)+35}{20}\Big) + \exp\Big(\frac{-\big(V(t)+35\big)}{20}\Big)}$$

In particular, α_x and β_x are the rates for channel activation and inactivation, depending on the membrane potential V_T. The terms $p_\infty(t)$ and $p_\tau(t)$ are the steady-state value and time constant for the slow potassium channel. So, these enhancements allow the model to capture the different firing patterns of FS, RSA and IB neurons, and intrinsically bursting behaviors, by tuning the related parameters [20].

Synaptic Transmission

Neurons exchange information through two distinct synaptic mechanisms: chemical and electrical transmission. These two modes of signal propagation coexist in all nervous systems [30] and each neuron can receive signals through both pathways. Looking closer, electrical synapses play a crucial role in synchronizing neural activity and differ from chemical synapses in terms of speed, directionality, and modulation capabilities. Their function is based on the almost simultaneous passage of electrical signals through the gap junctions, a sort of physical bridge between adjacent neurons that allows ions to flow between cells, and their role is particularly relevant in circuits that require fast and synchronized neuronal responses, such as those involved in breathing regulation and reflexive motor actions.

Unlike electrical synapses, chemical synapses communicate through a specific neurotransmitter, an action potential arrives at the pre-synaptic terminal and induces the release of neurotransmitters into the synaptic cleft. These chemical messengers bind to specific receptors in the post-synaptic neuron, leading to the generation of post-synaptic currents that modulate membrane potential and influence neuronal activity. The communication is therefore monodirectional (solely from presynaptic to post-synaptic neuron).

Since both electrical and chemical synapses play a crucial role in neural communication, it is necessary to incorporate them into a mathematical model. Thus, the following modifications to the membrane potential equation aim to integrate these two types of synaptic currents ensuring a more accurate representation of signal transmission.

So, as a final step, still according to [31, 32], we need to extend the membrane potential formula to include electrical I_{el} and chemical I_{ch} synaptic currents to fully adhere to the biology of signal transmission in human neurons.

For each neuron i, the final updated HH-extended equation turns out to be:

$$\begin{aligned}\frac{\delta V(t)}{\delta t} =& \frac{1}{C}\Big(I_{in}(t) - g_L\big(V(t)-E_L\big) - g_K n^4(t)\big(V(t)-E_K\big) - g_M p(t)\big(V(t)-E_K\big) + \\ &- g_{Na} m^3(t) h(t)\big(V(t)-E_{Na}\big) - g_{Ca} q^2(t) s(t)\big(V(t)-E_{Ca}\big) + I^i_{el} + I^i_{ch}\Big)\end{aligned} \tag{3}$$

The electrical synaptic current for a certain post-synaptic neuron i is defined as

$$I^i_{el} = \sum_{j=1}^{N} \overline{g}_{el} w^{el}_{i,j}\big(V_j(t-\tau) - V_i(t)\big), \tag{4}$$

where $\overline{g}_{el}$ is the maximal conductance and $w^{el}_{i,j}$ is the synaptic weight for the electrical connection from each presynaptic neuron j to the postsynaptic neuron i.
While the chemical synaptic current is defined as

$$\begin{aligned} I^i_{ch} &= \sum_{j=1}^{N} \overline{g}_{ch} w^{ch}_{i,j} r_j(t-\tau)\big(V^j_{syn} - V_i(t)\big), \text{ where} \\ \frac{\delta r(t)}{\delta t} &= \big(\frac{1}{\tau_{rise}} - \frac{1}{\tau_{decay}}\big)\frac{1 - r(t)}{1 + \exp\big(-V(t) - 20\big)} - \frac{1}{\tau_{decay}} r(t). \end{aligned} \tag{5}$$

The involved parameters are

- V^j_{syn}: a constant value representing the synaptic reversal potential of the synapse between the pre-synaptic neuron j and the post-synaptic neuron i, determined from experimental data and refined through optimization using genetic algorithms [32, 20]. This constant varies according to the type of neuron j, as shown in *Table* 1;

- $r_j(t-\tau)$: a function that represents the synaptic dynamics of the fraction of bound receptors, as described in [31]. Here, we set $\tau_{rise} = 0.5$ ms and $\tau_{decay} = 8$ ms to denote the synaptic rise and decay time constants, respectively. The parameter τ (in milliseconds) accounts for the transmission delay of information between neurons i and j. To reduce noise and simplify the analysis, we assume $\tau = 0$, corresponding to a regime in which neurons exhibit near-regular bursting activity [32].

A valuable example - Lateral Inhibition in Visual Processing

In a recent study, Giannari and Astolfi [21] proposed to model some optical illusions occurring in the visual system by defining a network where two only kinds of HH neurons are present, i.e., excitatory RSA neurons and inhibitory FS neurons, which act according to *Equation* 1 of the extended HH model. The effect is obtained by reproducing the action of the lateral inhibition, which enhances edge detection and contrast perception by selectively suppressing neighboring neural activity.
The authors proposed a model that successfully integrates both chemical and electrical synapses, providing a biologically and realistic simulation of neural networks. In particular, the electrical synapses enhance neural synchronization and contribute to network stability, while chemical synapses introduce a more precise modulation of neural activity, allowing both excitatory and inhibitory effects.

The topology of the defined network is feed forward and it consists of three distinct layers, where excitatory and inhibitory connections are mixed. The input to the network simulate different level of brightness in a visual stimulus. Analyzing the firing frequency of the output neurons, it has been assessed how lateral inhibition modulates their responses in relation to the amplitude of the current received by the input neurons. In this way, the authors compare the original input image processed by the neurons with the perceptual representation reconstructed by the brain after the effect of lateral inhibition.

Cells that fire together, wire together: Learning Rules in Hopfield Networks

In 1982, Dr.Hopfield published his work concerning collective properties of systems having a large number of simple equivalent components, already indicated as neurons [3]. The Hopfield model is one of the earliest examples of a recurrent network capable of functioning as an associative memory system. However, its original formulation does not fully align with the biological constraints observed in real neurons and synapses.

Each node of the network layers, referred to as a neuron since the first formulation, can assume only two possible states: $+1$ (active) or -1 (inactive). In the simplest formulation, the connections between neurons are symmetric and weighted by real positive values (i.e., $w_{ij} = w_{ji}$), furthermore, no self-connections are allowed (i.e., $w_{ii} = 0$) [3].

The information is stored in the neurons of the block layer, which act as memory cells. The model supports two main phases that mimic brain activity: a learning phase, during which weights are updated according to supervised examples, and a retrieval phase, in which the weights are considered stable, and memorized information is produced in response to an external input. The stored information, represented as patterns, benefits from connections weights, say synaptic strengths, that are modified according to the Hebbian rule [33] «cells that fire together, wire together» or, more clearly, «any two cells or systems of cells that are repeatedly active at the same time will tend to become associated, so that activity in one facilitates activity in the other(s)»[33].

As a consequence of the adoption of the Hebbian principle, neurons that belonging to the same pattern tent to behave similarly and their connections will enhance it by promoting higher values. On the other hand, neurons belonging to different patterns are discouraged from being active simultaneously, as their mutual interaction weaken.

Thus, a pattern μ can be considered as the snapshot of the activity of its N network's neurons at a given time. It can be represented as a vector of size N whose components are $\xi_1^{(\mu)}, \ldots, \xi_N^{(\mu)}$, with $\xi_i^{(\mu)} \in \{-1, 1\}$ being the activity of neuron i in the pattern μ. The number N will be also indicated as the size of the network.

The output of the Hopfield network is a sequence of patterns that evolve in time and that tent toward a stable configuration, called attractor [3]. The characteristics of the network, and in particular the assumption of a symmetric interaction between neurons, which is not fully adherent to the biological interactions as we will underline in *Section* 5, ensure the presence of stable configuration and convergence for any input.

The synaptic connections between neurons store the information of P patterns, and are arranged in a $N \times N$ matrix of synaptic weights $w_{i,j}$, for each couple of neurons i and j. These weights are set according to the Hebbian Rule:

$$w_{i,j}^{(\mathrm{HR})} = \frac{1}{N} \sum_{\mu=1}^{P} \xi_i^{(\mu)} \xi_j^{(\mu)}. \tag{6}$$

This simple rule is effective, but has two main limitations:

1. The presence of predominantly positive weights throughout the network, that may lead to weight saturation and consequently reduces memory capacity.

2. The assumption that all neurons are fully connected, which oversimplifies the sparse connectivity found in biological systems.

As a matter of fact, there is a mathematical limit to the storage capacity of the number of patterns P in the Hopfield network model that uses the Hebbian rule, as shown by Amit et al. in [34].
This limit can be set to αN, with $\alpha \cong 0.14$, and, as expected, acts by enhancing the number of pattern-retrieval errors on the space of the input patterns. A second relevant study by the same authors [35] explores the stability of output configurations when this limit is approached and exceeded.

The Willshaw Rule [36], which we will use in our model, refines the Hebbian learning rule by introducing control mechanisms that enhance both storage capacity and biological plausibility:

$$w_{i,j}^{(\mathrm{WR})} = \Theta\big(\sum_{\mu=1}^{P} \xi_i^{(\mu)} \xi_j^{(\mu)}\big) \tag{7}$$

where $\Theta(x)$ is the Heaviside function [37] that returns 1 for $x > 0$, 0 otherwise.
Unlike the Hebbian rule, in the Willshaw formulation the activity variable is defined as $\xi_i^{(\mu)} \in \{0, 1\}$, where $\xi_i^{(\mu)} = 1$ and $\xi_i^{(\mu)} = 0$ denote that neuron i is active or inactive in pattern μ, respectively. In this setting, we define the cardinality $|\mu|$ of the pattern μ as the number of its active neurons. Throughout the paper, we will denote it by the letter $M = |\mu|$. Synaptic weight $w_{i,j}$ is potentiated (set to 1) only when both neurons are active simultaneously in at least one pattern μ. This binary model simplifies the calculation compared to the original Hebbian formulation.

Hasegawa's Model: A Bridge Between HH and Hopfield Network

One of the first and most relevant attempts to develop a biologically plausible associative memory model, capable of efficiently storing and retrieving patterns while maintaining key properties of real neural networks, has been carried out by H. Hasegawa in [12]. It is noteworthy that this model yet constitutes a valuable tool to study associative memory networks and so it represents a benchmark of our study.
Hasegawa's network extends the traditional Hopfield framework incorporating 100 HH neurons, providing a bio-physically accurate description of neural activity based on ion channel dynamics. Unlike traditional models based only on firing rates, it emphasizes rigorous spike timing, making it a temporal coding network.

One of the main biological characteristics of the model is the use of HH neurons along with synaptic connections that reproduce both excitatory and inhibitory effects.
The network architecture is fully connected, without any modular or structured organization. Synaptic interactions are embedded in an equation that expresses the global interaction between neurons, without explicitly differentiate between chemical and electrical connections. Learning follows the classical Willshaw rule, allowing neuron-to-neuron connectivity that strengthens when pairs of neurons share at least one pattern.
The network is tested under both ideal and noisy conditions, including imperfect inputs and transmission delays, and demonstrates several key results, notably achieving a reasonably high storage capacity.

$$\alpha_c = \frac{P_{\max}}{N} \sim 0.4 - 2.4 \quad \text{for } f \sim 0.10 - 0.04, \tag{8}$$

Where f represents the average activity of the network, i.e., the fraction of neurons that are active in each pattern.
We emphasize that the storage capacity depends on the levels of neuronal activity, while the model exhibits robustness to temporal delays, successfully retrieving stored patterns despite variations in spike timing.
In the Hasegawa's model the critical capacity α_c adheres to the theoretical asymptotic growth $\alpha_c \propto -\log(f)/f$ (among others, see [38]).
Although the system maintains effective recall performance even when presented with partially correct inputs, and generally performs comparably to standard Hopfield networks, the use of associative memory models based on HH neurons remains limited due to their high computational cost.
Hasegawa's model also presents some relevant limitations that are substantially addressed in our research. We sketch them hereafter.

1. *Symmetric synaptic weights.* The use of symmetric synaptic weights deviates from biological reality. In real brain networks, plasticity is often asymmetric and governed by spike-timing-dependent mechanisms, which play a key role in learning and memory systems.

2. *Full connectivity.* The model assumes a full connected network, which does not reflect the sparse and modular architecture typically observed in real cortical circuits. This kind of connectivity can result in increased interference among patterns and reduced computational efficiency, especially as network size scales up.

3. *Simplified synaptic transmission.* In biological systems neurons communicate via both chemical and electrical synapses. Hasegawa's model omits this dual modality, leading to an oversimplified representation of neural communication and limiting the reproduction of key dynamics such as adaptation and bursting.

4. *Oversimplify inhibition.* In real neural circuits, inhibitory interneurons are highly distinct in terms of function and connectivity. This lack of diversity limits the model's ability to capture the role of inhibition in stabilizing activity and refining pattern separation.

5. *Fixed delays and uniform synaptic weights.* The model assumes fixed transmission delays and uniform synaptic strengths, while biological networks display heterogeneous delays and diverse plasticity profiles. These simplifications limit the model's ability to account for temporal coding and the rich dynamics of memory processing.

We believe that incorporating diverse inhibitory populations, and adopting more realistic connectivity patterns, would greatly enhance both its explanatory power and applicability to real neural systems.

3 A New Bio-Inspired Associative Memory Model

We present a biologically plausible model of associative memory that shows high performances in the storage and retrieval of patterns, overcoming some of the main issues of Hasegawa's model proposed in [12].
This model, described in detail in the following section, extends the traditional Hopfield networks while preserving the capabilities of pattern storage and retrieval. In particular, it incorporate dynamic neural interactions that evolve over time according to the chaining internal starers of the neurons. This characteristic is obtained by relying on the *recurrence* property of the Hopfield networks that consider mutual interactions among the neuron blocks located in the block layer. Such a characteristic allows us to better capture the time dependent nature of neural activity and synaptic transmission, making the model biologically realistic.
In contrast, the synaptic weights between blocks are static over time and serve to store patterns within the network.
Let us start the detailed description of our network model by introducing both the network topology and the synaptic connections that support the storage and retrieval of patterns.

Network Topology

Following the Hopfield structure, the neurons are arranged into three layers:

Input layer —> where sensory and motor input neurons, typically IB ones, are located. Each neuron is responsible for receiving an input signal in the form of a single spike from the environment and propagated it inside the network. After such initial activity, the IB neurons remain silent until the arrival of the next input.

Block layer —> composed of blocks of neurons. Each block receives input from an IB neuron and consists of three neurons, two RSA and one FS, connected as shown in *Figure* 1. The FS neuron modulates activity between blocks to maintain network stability and reduce interference through backward inhibition, producing lateral inhibition.

Output layer —> composed of RSA neurons whose role is to acquire the neuron activities output from each block, they represent the network's state over time.

Let N the size of the network. The input and output layers contain $B = N/5$ neurons each, while the block layer is composed by B 3-neurons blocks. The intra-layer and inter-layer connectivity follows a structured pattern designed to ensure both efficient signal transmission and network stability. These interactions are governed by *Equation* 3, in accordance with the types of neurons involved.

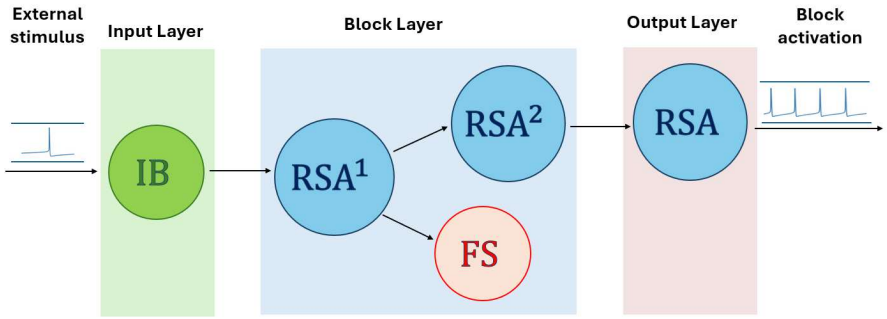


Figure 1: Representation of a single neural block structure along with its input and output interactions. From the left: a single spike current, as part of an external stimulus, reaches an IB neuron in the Input Layer that actives the RSA^1 neuron of the block. RSA^1 transmits the signal to both RSA^2 and FS inhibitory neuron through electrical synapses Finally, the RSA^2 transits its activity to the RSA neuron of the output layer, on the right, over time.

In particular the connections are defined as follows, see *Figure* 2:
For each $1 \leq i \leq B$,

- The input neuron IB_i transmits a single spike, it represents part of a full external stimulus (i.e., an initial pattern) to the first excitatory RSA_i^1 neuron of i-th block in the block layer through an electrical synapses, in order to start the initial excitation.
- An excitatory electric signal is then propagated from RSA_i^1 to the other two neurons within the i-th block, RSA_i^2 and FS_i.
- A backward propagated excitatory chemical signal is sent from RSA_i^2 to the outer RSA_j^1 neurons of the other blocks, with $1 \leq j \leq B$, $j \neq i$. It creates an excitatory feedback loop that relies the excitatory part of the Willshaw rule by setting higher weights when i and j belong to the same stored pattern(s).
- In parallel, a chemical inhibitory signal moves back from FS_i to the outer RSA_j^1 and FS_j neurons of all other blocks, with $1 \leq j \leq B$, $j \neq i$. Notably, the FS_i inhibitory actions on the other inhibitory neurons preserve or inhibit their activities, a mechanism known as *disinhibition*. It is here where we create a feedback loop that realizes the inhibitory part of the Willshaw rule preventing the activities of the blocks not sharing a common pattern with block i.
- Finally, the activity of RSA_i^2 is transmitted to the output layer neuron RSA_i, thereby presenting, instant by instant, the pattern induced by the input.

The network's synaptic values are stored in two sparse matrices. *Ael* for electric synapses and *Ach* for chemical synapses, both of size $N \times N$. While constant synaptic values are often assumed, as detailed below, we choose to store them in matrices for generality. This design choice does not significantly affect the performances of the network.

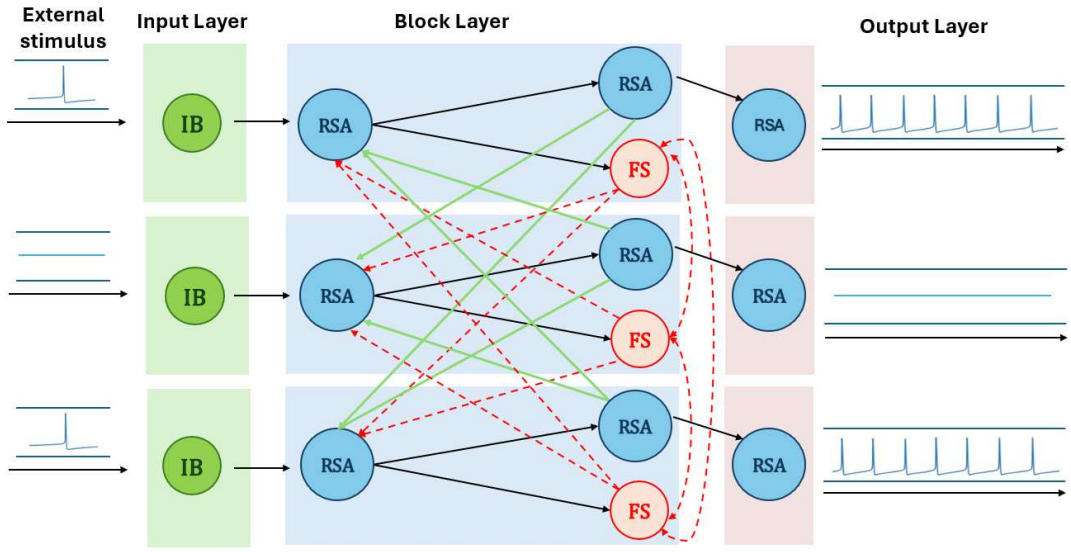


Figure 2: An example of network's connections for three blocks ($B = 3$, $N = 15$). The three layers (Input Layer, Block Layer and Output Layer) are highlighted in different colors. Electrical and chemical excitatory synapses are represented by black and green arrows, respectively, while inhibitory chemical synapses are shown as dashes red arrows. Inter-block connectivity is regulated by synaptic matrices derived by the Willshaw rule. In particular, FS neurons, through lateral inhibition mechanism, act (i) on the RSA^1 neurons of the other blocks as a stabilizing factor of the network, (ii) on the other FS inhibitory neurons to perform a disinhibition action by reducing their inhibitory effect. The Output layer reflect the spiking activity of RSA^2 neurons, exhibiting the firing dynamics of each block.

Each block can be regarded as a single computational unit, aggregating information from its constituent neurons and contributes to the final activation pattern provided by the network.
This design choice ensures a more structured and biologically relevant approach to associative memory processing, resembling the columnar organization observed in the neocortex. Indeed, in biological systems, information is often processed at the level of local neuronal assemblies rather than through individual neurons. We underline that the block-based structure facilitates noise reduction, enhances memory stability, and enables parallel processing of stored patterns.

Synaptic Architecture

A fundamental feature of our network is the implementation of the *lateral inhibition* mechanism which plays a key role in improving memory recall by reducing interference among stored patterns [39]. When a specific pattern is recalled, FS neurons suppress competing activations, ensuring that there is no interference from the other stored patterns, which could minimize spurious activations and interfere with the efficiency of the associative recall task. In addition, we incorporated the mechanism of *disinhibition*. Specifically, FS neurons not only inhibit excitatory RSA neurons in other blocks, but are also interconnected through inhibitory FS–FS synapses. These setup allows

one FS neuron to suppress the activity of another FS neuron, effectively decreasing inhibition on specific blocks. Disinhibition occurs when inhibition is reduced or temporarily eliminated [40].
At the beginning of the process, an external current is applied to IB neurons to simulate input from external sources, such as sensory signals or other neural stimuli. Without these, neurons remain in a quiescent state.
To assess the activation of the i-th block, we monitor the spike timings of neuron RSA_i, which projects to the output neuron RSA_i^2. A spike is recorded when the membrane potential $V(t)$ exceeds 0.0 mV. The temporal distribution of these spike events is then used to evaluate both the functional behavior of the network and the effectiveness of the connectivity design. For each output neuron RSA_i^2, we obtain an array of m spike times:

$$\mathrm{ST}_i = [t_1, t_2, ..., t_m]$$

Connections between block layer follow biological inspired rules, with distinct mechanisms for excitatory RSA and inhibitory FS neurons.
Excitatory chemical synapses from RSA_i^2 to RSA_j neurons, with $i \neq j$ (green arrows in *Figure* 2), are stored in the matrix $A_{ch}(x, y)$, where x and y are two network's neurons, and follow the Willshaw rule in *Equation* 7 weighted by an interaction parameter $g_{\text{RSA-RSA}}$:

$$A_{ch}(\mathrm{RSA}_i^2, \mathrm{RSA}_j) = g_{\text{RSA-RSA}} \cdot w_{i,j}^{(\mathrm{WR})}. \tag{9}$$

Inhibitory chemical synapses from FS_i to RSA_j^2 neurons are defined by an inverse Willshaw rule, weighted by $g_{\text{FS-RSA}}$. This formulation ensures that inhibition is strongest where excitatory connectivity is weak, mirroring inhibitory balance mechanisms found in biological circuits:

$$A_{ch}(\mathrm{FS}_i, \mathrm{RSA}_j^2) = g_{\text{FS-RSA}} \cdot (1 - w_{i,j}^{(\mathrm{WR})}). \tag{10}$$

Each FS neuron is also responsible for the disinhibition process pushing inhibition on the FS neurons of the other blocks. This action is modeled as a constant connection, so that:

$$A_{ch}(\mathrm{FS}_i, \mathrm{FS}_j) = g_{\text{FS-FS}}. \tag{11}$$

Note that the matrix A_{ch} is not symmetric since the connections have a preferred direction. The parameters $g_{\text{RSA-RSA}}$, $g_{\text{FS-RSA}}$ e $g_{\text{FS-FS}}$ were determined through a brute-force search, systematically exploring a predefined parameter space to identify optimal values. This approach was necessary due to the high-dimensional and nonlinear nature of the system, which prevents direct analytical solutions. The selection criteria included network stability (avoiding uncontrolled excitation), biologically plausible firing behavior, and a balanced interplay between excitation and inhibition. After evaluating the effects of various parameter combinations, the following values were selected as optimal for ensuring robust and efficient network dynamics:

$$g_{\text{RSA-RSA}} = 0.03 \qquad g_{\text{FS-RSA}} = 1.2 \qquad g_{\text{FS-FS}} = 0.003 \tag{12}$$

Within the i-th block, the neuron RSA_i^1 forms electrical connections with both RSA_i^2 and FS_i. In addition, the input neuron IB_i projects to RSA_i^1 via an electrical synapse, and RSA_i^2 transmits its activity to the output neuron RSA_i of the same block through another electrical connection. All these electrical synapses are stored in the matrix A_{el} and assigned a constant weight of 0.2. We adopt a sparse and uniform configuration for A_{el} to allow for future generalization without significantly

increasing computational complexity. Electrical synapses are illustrated as black directed edges in *Figures* 1, 2.
In real neural systems, excessive excitation can destabilize network activity, potentially leading to uncontrolled firing and the accumulation of noise [41]. To counteract this, inhibitory neurons provide a feedback mechanism that regulates global network dynamics and prevents any single block from becoming overactive [42]. To replicate this biological principle in the model, all FS neurons are interconnected, avoiding self-connections, according to *Formula* 11, thereby enabling global inhibition across blocks.

Time-Dependent Overlap

Once the synaptic weights have been computed using P randomly generated patterns of the same cardinality, an initial stimulus ζ is provided to the network. This input acts as a cue to trigger the recall process, allowing the system to retrieve the most relevant stored pattern through associative memory dynamics. The response of the network is then assessed by monitoring the activation of output neurons to ensure correct pattern detection. To quantify retrieval accuracy over time, we introduce the time-dependent overlap parameter $m_\mu(t)$:

$$\begin{aligned} m_\mu(t) &= \frac{1}{B}\sum_{i=1}^{B}\left[2\xi_i^{(\mu)}-1\right]\left[2\eta_i(t)-1\right], \text{ with} \\ \eta_i(t) &= \begin{cases} 1, & \text{for } t \in [t_{im}-\delta t, t_{im}+\delta t] \\ 0, & \text{otherwise} \end{cases} \end{aligned} \tag{13}$$

The parameters are defined as follows:
- B: total number of blocks;
- $\xi_i^{(\mu)}$: state of the output neuron RSA_i in the stored pattern μ (0 for quiescent, 1 for active);
- t_{im}: time of the m-th activation of block i, determined by the firing of its associated output neuron RSA_i
- δt: temporal margin around spikes ($\sim 7\,\text{ms}$) that reflects the absolute refractory period of a neuron in the HH model.

If $m_\mu(t) = 1$, the temporal output perfectly matches the stored pattern μ, instead, decreasing values of $m_\mu(t)$ indicate that the retrieval of the pattern is failing, until reaching -1 that denotes the perfect mismatch of the two input and output patterns.
We emphasize the introduction of a time window δt, which accounts for synaptic delays and temporal variability. In biological neural systems, each spike requires a finite time to propagate and influence downstream neurons, and spikes across different neurons rarely occur simultaneously. Instead, they are distributed within a short temporal interval. The window δt captures this intrinsic variability, allowing for a more biologically plausible evaluation of spike coincidence.
In the following analysis, we consider retrieval to be successful when the overlap reaches $m(t) = 1.0$ at $t \gtrsim 40$ ms.

4 Results and Discussion

In this section, we analyze the pattern retrieval capability and storage capacity of our model. By investigating the system's response to input patterns under varying memory loads, we aim

at quantifying its retrieval efficiency and comparing its performance with the model presented by H.Hasegawa in [12].
We assess the network's behavior when presented an initial stimulus ζ that perfectly matches one of the stored patterns μ, referred to as a *perfect input*, and also examine its ability to maintain accurate recall as the number of stored patterns increases.
We measure retrieval success through time-dependent overlap functions and spike activity, allowing us to determine the conditions under which stored patterns can be accurately retrieved. We assume that, at the initial time t_0, all neurons start from the same biologically plausible state:

$$V(t_0) = -70, \qquad n(t_0) = m(t_0) = h(t_0) = p(t_0) = q(t_0) = s(t_0) = r(t_0) = 0. \tag{14}$$

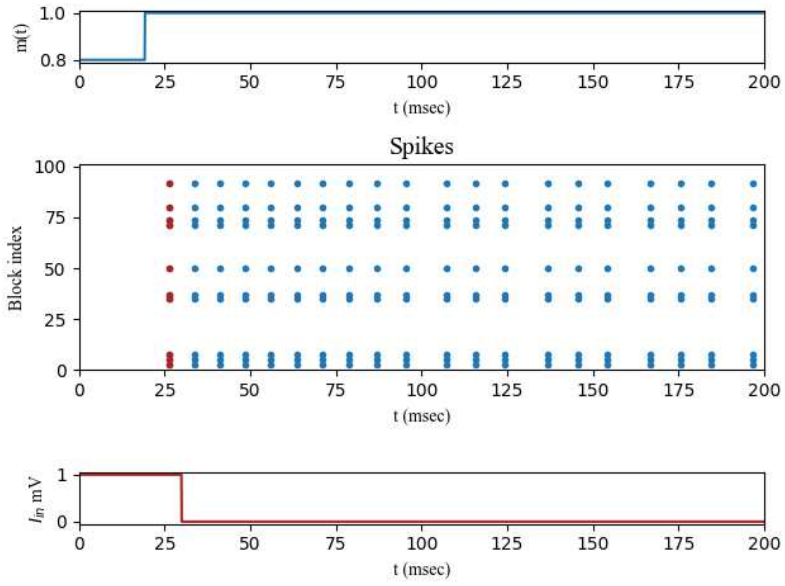


Figure 3: Successful pattern retrieval with a perfect input. The network has $B = 100$ blocks and stores $P = 70$ patterns, with $M = |\mu| = 10$ active blocks per pattern (i.e., $f = 0.1$). The top graph shows the time-dependent overlap $m(t)$, highlighting the network's ability to retrieve and sustain a stored pattern over time. The middle graph displays the spiking activity of each block over 200 ms window: each light blue dot represents a spike from a block's output RSA neuron. The ordered and repetitive spiking pattern reflects the recognition of the perfect input pattern μ (marked by red dots) stored in memory. The bottom graph shows the input current I_{in} (red line), the external stimulus which is applied to the input layer until $t = 30$ ms and then removed. Despite this brief initial stimulation with an external current, the network is able to maintain a robust internal state of activation, highlighting its capacity for persistent and selective memory retrieval under noise-free conditions.

Figure 3 shows a successful retrieval response of our network model to a perfect input that produces the time-dependent overlap $m(t) = 1.0$. The network's characteristics and the parameters' values are detailed in the caption.

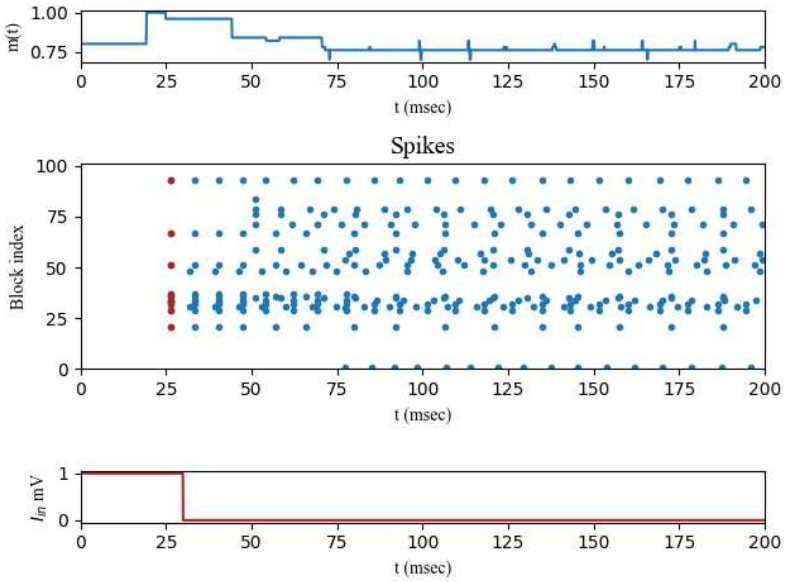


Figure 4: Failed pattern retrieval under high memory load. The network consists of $B = 100$ blocks and stores $P = 120$ patterns, with $M = 10$ active blocks per pattern (i.e., $f = 0.1$). The top panel shows the the time-dependent overlap $m(t)$, which quantifies the similarity between the current network state and the target pattern. A rapid drop from 1.0 indicates a failure to maintain the recall after the stimulus is removed. The middle panel illustrates the spiking activity of all output blocks over time: each point represents a spike event from the RSA neurons of a block. The disorganized and non-selective fire model illustrates a loss of coherence and specificity in network response. The bottom panel shows the external input current I_{in}, which is applied at $t = 0$ ms and turned off at $t = 30$ ms. Despite the perfect initial stimulus ($\zeta = \mu$), the network fails to recover and maintain the correct memory trace due to overload, reveling its capacity limitations.

To refine the performance of the model, we introduce the notion of *storage capacity* of a network, defined as $\alpha = P/N$, where P is the number of stored patterns and N is the size of the network. In our framework, we replace N by the number of blocks B in the block layer, since each block contributes as a single unit to the pattern (as already underlined, the contribution of each block is passed and so detected by the corresponding output neuron).
We say that a network has a storage capacity α when, on successive loads of P patterns, the correctly retrieved number of patterns over the total number of presented patterns tents to one, as the number of these last increases.
We denote by $\alpha_c = P_{max}/N$ the *storage capacity limit* of a network, i.e., the maximum value (experimentally obtained) of its storage capacity. In *Figure* 4, an example is shown where too many patterns ($P = 120$, $M = 10$) are memorized in the network, consequently, the network struggles and fails to reconstruct a provided perfect input stimulus. The network parameters and characteristics are detailed in the caption.
Figures 3, 4 illustrate the transition between functional and non-functional memory retrieval in two model of the same size, highlighting the constraints imposed by the network architecture and

synaptic learning rules.
Classically, storage capacity is studied by analyzing how successful recall scales with the fraction of neuronal activity $f = M/N$ (or $f = M/B$ in our framework).
The capacity limits of our model are illustrated in *Figure* 5 both in terms of the maximum number of stored patterns P as a function of their common cardinality M and in terms of the value α_c as a function of f. A comparison with the maximum storage capacity of the Hasegawa's model is also provided.

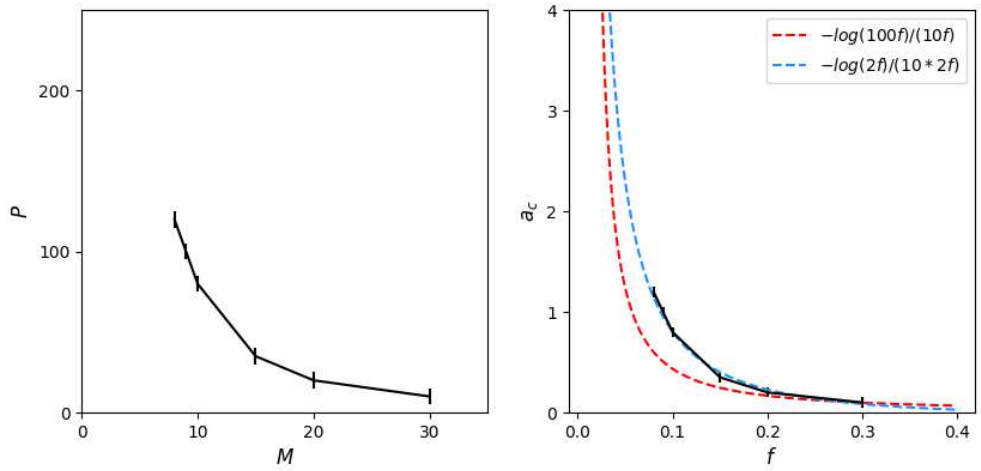


Figure 5: On the left: maximum number of patterns that can be stored in our network and correctly retrieved as a function of the (common) number of active neurons in each pattern. On the right: the same result in terms of the maximum storage capacity α_c, as a function of the fraction of active neurons f in each pattern. The black markers show the empirical results from our model with a network of $B = 100$ blocks (500 neurons), confirmed across different network sizes. On the right: the blue dashed line represents the approximation $\alpha_c = -\log(2f)/(10 \cdot 2f)$. The red dashed line corresponds to the maximum capacity function derived from Hasegawa's study.

We emphasize that both the Hasegawa model and ours adhere to the theoretical maximum storage capacity limit $\alpha_c \propto -\log(f)/f$, as shown, among others, in [38] and [43], and more recently confirmed in [44].
We underline that in all these studies, patterns belonging to the same memory load μ have a fixed common cardinality, with active neurons chosen randomly. It is worth noting that the maximum storage capacity decreases when patterns of different sizes are stored together [38].
We set the ground to present a final, comprehensive comparison between the H.Hasegawa's network and our model in terms of biological plausibility, performance, and storage capacity. Similarities and key differences are summarized in *Table* 2 and discussed below:

- The underlying synaptic organizations of the networks differ, while Hasegawa's model employs a fully connected topology, our approach propose a modular connectivity structure that supports memory segregation and reduces pattern interference. This design has biological relevance, as it resembles the columnar organization of the neocortex, which processes in-

formation through local neuronal assemblies rather than individual neurons. We emphasize that the block-based architecture promotes redundancy, which facilitates noise reduction and memory stability, while also enabling parallel processing of stored patterns.

- Hasegawa's model is based solely on an internal current that simulates neuronal interactions, whereas our model incorporates both electrical synapses within modular blocks and chemical synapses between blocks. The inclusion of electrical synapses (gap junctions) in our model offers a key advantage in promoting synchronization and rapid signal propagation. These synapses enhance neural coordination and increase the robustness of pattern retrieval, features not explicitly considered in H.Hasegawa's approach. The interplay between fast electrical transmission and slower, modulated chemical synaptic interactions allows our model to more accurately capture biologically relevant network dynamics.

- The mechanism of lateral inhibition plays a central role in memory retrieval and is more effective at suppressing undesired activations of blocks not involved in the target pattern, compared to the global constant inhibition employed in the H.Hasegawa's model. Even in cases of partial or imperfect input, lateral inhibition dynamically suppresses the spiking activity of irrelevant blocks over time, and prevents inappropriate inhibition through a disinhibition process. As a result, memory integrity is preserved, spurious activations are reduced, and the network becomes more efficient in associative recall tasks.

- The model proposed by H.Hasegawa is characterized by a maximum storage capacity function of the form $\alpha_c^H = -\log(100f)/10f$. It should be noted that no explicit criterion for setting this storage limit is provided. The expression follows the same theoretical dependency $\alpha_c \propto -\log(f)/f$ as our model, but with a lower scaling factor. In contrast, our network slightly outperforms H.Hasegawa's across the tested range of f, reaching a capacity of $\alpha_c = -\log(2f)/(10 \cdot 2f)$.

  For example, when $f = 0.1$, H.Hasegawa's network achieves a storage limit of $\alpha_c^H \approx 0.4$, whereas our model reaches $\alpha_c \approx 0.7$.

- The pattern retrieval process takes around 13 ± 5 seconds on a 500-neuron network governed by the related Willshaw rule with 70 stored patterns, while H.Hasegawa does not provide any information on time complexity. Despite the computational complexity associated with the HH type model, our network achieves high and efficient performance: 100 blocks simulate biologically accurate dynamics between neurons and complete a full pattern retrieval cycle in approximately 13 seconds. We consider it a notable result, since we have integrated some of the most common synaptic interactions into each other. A more detailed analysis is provided later in this section.

In summary, while both models align with the theoretical predictions of associative memory storage capacity, our biologically plausible, block-based architecture, incorporating both chemical and electrical synapses, demonstrates a more efficient and robust associative memory for pattern storage and retrieval. These results underscore the significant impact of biologically inspired constraints on neural network performance, suggesting that modularity and lateral inhibition play crucial roles in optimizing associative memory in realistic neuronal systems.

Key Features	Proposed Model	Hasegawa's Network
Neuron types	Hodgkin-Huxley neurons of three kinds: IB (excitatory), RSA (adaptive excitatory), FS (inhibitory)	Uniform Hodgkin-Huxley neurons without functional differentiation
Neuron roles	Each type plays a specific role: IB for input, RSA for signal integration, FS for inhibition	All neurons function identically
Network structure	Modular, block-based architecture (5 neurons per block), mimicking cortical microcircuits	Single-layer fully connected network
Inhibition mechanism	Explicitly implemented via FS neurons using inhibitory chemical synapses (inverse Willshaw rule)	Uniform inhibitory term applied directly in the membrane potential equation
Synapse types	Both electrical (within-block) and chemical (inter-block) synapses	Generic internal current that simulates neuronal interactions
Synaptic learning	Willshaw learning rule for chemical synapses and its inverse for inhibition	Classical Willshaw rule
Synaptic topology	Fixed intra-block connectivity via electrical synapses, inter-block weights learned	Fully connected synaptic matrix
Storage capacity	Achieves $\alpha_c \approx 0.7$ with 100 blocks at $f = 0.1$ (perfect input)	Achieves $\alpha_c \approx 0.4$ with 100 neurons at $f = 0.1$, more sensitive to imperfect inputs
Time complexity	The pattern retrieval process takes around 13 ± 5 seconds on a 500 neurons network governed by the related Willshaw rule	No time complexity has been provided

Table 2: Comparison between our proposed model and Hasegawa's HH-based associative memory network.

4.1 Comparison with other models

We decided to stress the comparison between the computational performance of our model with other well-known models in literature. The *Izhikevich model* [19], known for its mathematical simplicity but very low biological fidelity (it has only two differential equations), can simulate thousands of neurons in a real-time standard CPU. His model, due to the over-simplification of the ion dynamics and the absence of electrical and chemical synapses, is not suited for studies that require a detailed reproduction of neurobiological processes, so we choose to exclude it in our model. The *Leaky Integrate-and-Fire* (LIF) model [45] is, like Izhikevich model, extremely simplified: it considers only one differential equation to describe membrane potential dynamics, and it lacks the ability to reproduce biologically accurate firing patterns and channel-based membrane conductance. Again its performances on hundreds of neurons almost reach the real time: as an example simulating 500 LIF neurons for 200ms typically takes less than 0.5 seconds on a standard CPU. Synaptic inputs are normally modeled as current injections, without conductance dynamics or synaptic delays.

Consequently, its biological fidelity is considered very low.
Although it does not explicitly model ionic currents, a more biologically accurate model is *Adaptive Exponential Integrate-and-Fire* (AdEx) defined in [46]. The authors introduce non-linearity and adaptation currents, offering an intermediate compromise between realism and efficiency. The model is composed of two couple of differential equations, and is capable of reproducing several cortical firing patterns. The simulation time for 500 AdEx neurons over 200 ms is typically in the range of $1 - 3$ seconds.
Originally developed for muscle fibers, *Morris–Lecar model* [47] simulates membrane excitability using two couple of differential equations. It includes voltage-dependent Ca+ and K+ channels but it does not intrinsically generate fast action potentials due to the lack of Na+ channels. A typical simulation of 500 Morris–Lecar neurons over 200 milliseconds requires approximately 2 to 5 seconds, depending on numerical integration settings
In contrast, the HH model provides a well-detailed neuro-physical representation of membrane dynamics but a significantly higher computational cost. According to benchmarks conducted using the *Brian2 simulator* [48] simulation of 1000 HH neurons for 1 second may require several minutes on a standard CPU without GPU acceleration due to the stiffness of the system and the need to solve multiple non-linear differential equations per neuron. Even if we use a modest-scale simulation (for example, 500 neurons for 200 ms), the time required is approximately between $10 - 60$ seconds and depends on the complexity of the model and the optimization of the code [48].
Despite biological complexity (as stated previously, we use the complex *Equation* (3) on 500 HH-extended neurons), our network completes a full pattern retrieval cycle in about 13 ± 5 seconds. If compared, this reflect a notable computational efficiency.
Table 3 provides a quantitative comparison of the models, while *Figure* 6 show the results from a pure qualitative perspective.

Model	**ODEs**	**Synapses**	**Time**	**Use Case**
LIF	1	None or basic	<0.5 s	Large-scale simulations
Izhikevich	2 + reset	None	<1 s	Real-time spiking behavior
AdEx	2	No ionic dynamics	∼1–3 s	Cortical modeling
Morris–Lecar	2	No spikes/synapses	∼2–5 s	Excitability modeling
Hodgkin–Huxley	4	Optional	10–60 s	Biophysical modeling
Our model	8	Chem. + Electr.	**∼13 s**	Associative memory

Table 3: Comparison among common spiking neuron models. ODEs values consider the number of differential equations of the model. This parameter can be thought as related to its complexity. Synapses show the adequacy of the model to the biological characteristics of the neurons' activity. Time provides the average time or the time interval when simulating 200 ms of ~ 500 neurons. Use Case indicates possible application frameworks of each model.

5 Conclusions

We have presented an associative memory model that constitutes an integrated approach that bridges abstract theoretical store-and-retrieval Hopfield networks with biologically realistic neural dynamics. The proposed model aims to overcame some limitations still present in recent associative models that rely on a forerunner one defined by H.Hasegawa in [12].

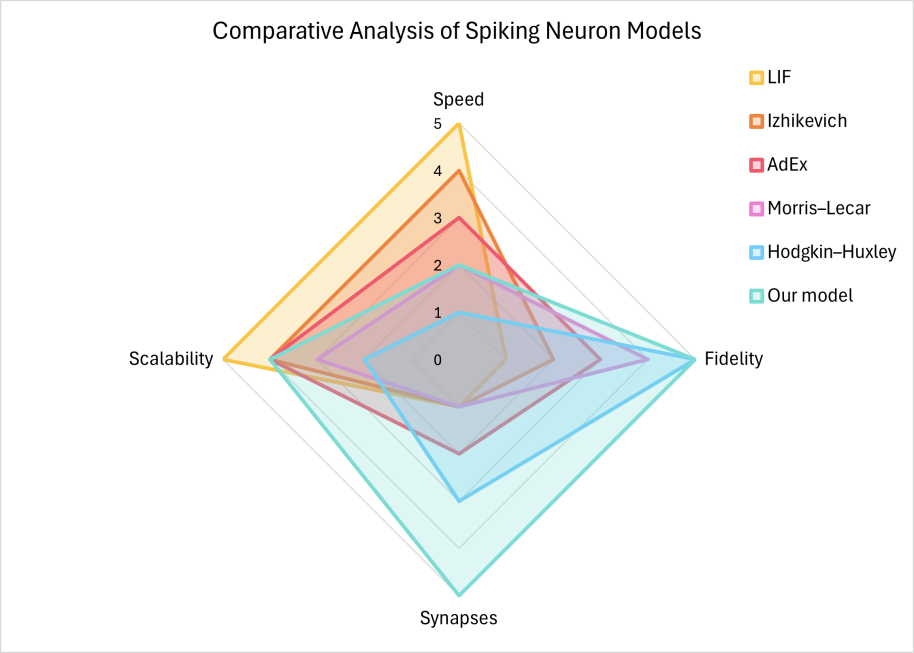


Figure 6: An immediate qualitative comparative analysis of the main characteristics of the six models presented in *Table* 3: simulation speed, biological fidelity, synaptic realism, and scalability. Each feature is rated on a scale from 1 (very poor or very slow) to 5 (high fidelity or very fast). This figure provides an intuitive overview of the trade-offs involved in choosing between simplified and biologically detailed models.

In particular, we modeled the activity of each single neuron using the *Equation* (3), which refine the HH neuron behavior incorporating membrane potential dynamics along with mutual chemical and electrical interactions, providing a much stronger biological plausibility.
While the HH model provides a biophysically grounded description of different neuron classes, it does not explicitly model synaptic interactions. To simulate large neural networks over time, many studies simplify these equations or adopt simpler network topologies, trading off biological detail for computational tractability. A major limitation of the HH-extended equation is its high computational cost, that dramatically increases in case of fully connected networks where presynaptic influence scales over time [49], restricting simulations to relatively small networks.
A further challenge in associative memory models is the interference caused by overlapping patterns, when some neurons participate in multiple stored patterns, potentially disrupting correct retrieval. In [12], H.Hasegawa addressed this issue with a global constant inhibition acting on all neurons, a mechanism lacking clear biological support.
In contrast, our approach replaces single neurons with modular blocks, each containing excitatory and inhibitory neurons that interact via chemical and electrical synapses. We implement local inter-block lateral inhibition through FS inhibitory neurons, combined with disinhibition mechanisms that dynamically modulate excitation-inhibition balance. This design avoid the fully connectedness of the network, so enhancing biological plausibility and improves pattern separation, reducing

interference more effectively than global inhibition.
Within blocks, we use the Willshaw learning rule to modulate chemical synapses, reinforcing stable pattern storage and retrieval. This biologically inspired synaptic plasticity further supports robust memory performance.
A final relevant aspect of our model lies in its maximum storage capacity, α_c. While both H. Hasegawa-like models and our model follow the theoretical asymptotic behavior $\alpha_c \propto -\log(f)/f$, we observed higher performance as the mean number of active neurons per pattern decreased, as shown in *Figure* 5.
In summary, our approach employs graph theory and computational optimization techniques to efficiently model large-scale neural networks. By integrating the inverse Willshaw rule with temporal overlap measures, the model captures key features of biological neural systems, including the balance of excitation and inhibition, noise suppression, and the critical role of precise timing in both encoding and retrieval.
Looking ahead, we plan to expand the model to incorporate a broader range of neuronal types, additional synaptic mechanisms and more complex network architectures. These improvements will enhance its relevance and applicability in both theoretical and applied neuroscience.
Nevertheless, the model offers valuable insights into the mechanisms underlying learning and memory: explores new dimensions concerning the interaction between memory formation and neural activity and provides a strong foundation for investigating fundamental questions in neuroscience, such as how neural circuits encode and retrieve information and the specific roles of inhibitory and excitatory neurons in maintaining stability and functionality within networks. After all, our model represents a step forward in the study of brain circuits: thanks to its adaptability, based on biological principles, the model provides a step forward to advance our understanding of the brain. In the meanwhile, its structure opens the door to practical applications in brain-inspired computation.

Limitations and Future Perspectives

Despite its strengths, the model presents several biological limitations that warrant further investigation. One notable drawback is the assumption of constant synaptic weights. Incorporating different weight updates, such as spike-timing-dependent plasticity (STDP) or activity-dependent synaptic scaling, could enhance the biological realism of the model.
Another limitation lies in the high connectivity of the block layer, which deviates from the sparse and modular connectivity observed in biological neural circuits. Future work aims to implement more selective, modular connectivity patterns inspired by cortical architectures to improve computational efficiency and more accurately reflect real brain networks.
Additionally, our work thus far has focused exclusively on perfect pattern inputs. A key future objective is to systematically evaluate the network's pattern recognition capabilities under imperfect conditions. This includes input patterns with partial overlap or the presence of competing memories. Such an analysis, based on the overlap measure described in *Section* 3, aims to identify the critical threshold beyond which the network fails to reliably retrieve stored information. While Hasegawa's study provides a preliminary qualitative exploration of this problem, a more rigorous and quantitative approach is needed to fully characterize the model's memory resolution and robustness.
Another important aspect concerns the stability of network dynamics. Unlike classical Hopfield networks, our model lacks formal convergence guarantees due to the inclusion of asymmetric interactions and nonlinear time-dependent synaptic responses. However, all numerical simulations

have consistently shown convergence to stable configurations, suggesting the presence of an intrinsic self-stabilizing behavior, a property we intend to investigate more thoroughly in future work.
Beyond theoretical development, the model shows potential for practical applications in both neuroscience and artificial intelligence. In neuroscience, it could help simulate circuit-level effects of neurodegenerative diseases such as Alzheimer's and Parkinson's, offering insights into memory decline and possible interventions. In artificial intelligence, its biologically inspired learning rules and modular architecture make it a promising foundation for neuromorphic systems with more adaptive and efficient learning capabilities.
In conclusion, the proposed model successfully captures key features of associative memory and neural computation with high efficiency. Future developments will build upon this solid foundation by incorporating more complex connectivity patterns, adaptive learning mechanisms and empirical validation, thereby enhancing both its biological realism and its applicability to neuroscience and artificial intelligence challenges.

Simulation Environment

All simulations were carried out on a Windows 11 Pro system equipped with an Intel® Core™ $i7 - 14700$ processor, 32 GB of RAM, and an AMD Radeon RX 7800 XT GPU. The simulation code was implemented in Python 3.12.1 and used the following libraries: NumPy ($v1.26.4$), SciPy ($v1.13.0$), and Matplotlib ($v3.8.4$) for numerical integration, signal processing, and data visualization, respectively. A fixed integration timestep of 0.01 ms was employed to ensure numerical stability during the simulation of HH based neuronal dynamics. The source code is available upon reasonable request by email and may be shared for academic review and viewing purposes only.

Declaration of Competing Interest

The authors state that they have no financial conflicts of interest or personal connections that might have influenced the research presented in this paper. No funding are requested for this research. All authors have read and agreed to the published version of the manuscript.

Author contributions: CRediT

Diletta Bartolini: Conceptualization, Software
Miranda Bellezza: Conceptualization, Formal analysis, Software, Validation, Writing – original draft, Writing – review and editing
Azzurra di Palma: Conceptualization, Formal analysis, Methodology, Validation, Writing – original draft, Writing – review and editing
Andrea Frosini: Conceptualization, Formal analysis, Software, Writing – original draft, Writing – review and editing, Supervision, Project administration
Vincent Pelletier: Conceptualization, Software

References

[1] J. R. Anderson and G. H. Bower, *Human Associative Memory*. Psychology Press, 1974. 2

[2] T. Kohonen, *Self-organization and associative memory*, vol. 8. Springer Science & Business Media, 2012. 2

[3] J. Hopfield, "Neural networks and physical systems with emergent collective computational abilities," *Proceedings of the national academy of sciences*, vol. 79.8, pp. 2554–2558, 1982. 2, 9

[4] S. Thorpe, D. Fize, and C. Marlot, "Speed of processing in the human visual system," *nature*, vol. 381, no. 6582, pp. 520–522, 1996. 2

[5] C. Stöckl and W. Maass, "Optimized spiking neurons can classify images with high accuracy through temporal coding with two spikes," *Nature Machine Intelligence*, vol. 3, no. 3, pp. 230–238, 2021. 2

[6] S. Betteti, G. Baggio, F. Bullo, and S. Zampieri, "Input-driven dynamics for robust memory retrieval in hopfield networks," *arXiv preprint arXiv:2411.05849*, 2024. 2

[7] J. Y.-C. Hu, T. Lin, Z. Song, and H. Liu, "On computational limits of modern hopfield models: A fine-grained complexity analysis," *arXiv preprint arXiv:2402.04520*, 2024. 2

[8] R. Mtenga, M. Bode, and R. Khalil, "Do not let the beginning trap you! on inhibition, associative creative chains, and hopfield neural networks," *The Journal of Creative Behavior*, 2023. 2

[9] G. Kim and P. Kim, "Selective inhibition in ca3: A mechanism for stable pattern completion through heterosynaptic plasticity," *bioRxiv*, pp. 2024–08, 2024. 2

[10] V. Folli, M. Leonetti, and G. Ruocco, "On the maximum storage capacity of the hopfield model," *Frontiers in computational neuroscience*, vol. 10, p. 144, 2017. 2

[11] G. Gosti, V. Folli, M. Leonetti, and G. Ruocco, "Beyond the maximum storage capacity limit in hopfield recurrent neural networks," *Entropy*, vol. 21, no. 8, p. 726, 2019. 2

[12] H. Hasegawa, "An associative memory of hodgkin–huxley neuron networks with willshaw-type synaptic couplings," *Journal of the Physical Society of Japan*, vol. 70, no. 7, pp. 2210–2219, 2001. 2, 3, 10, 12, 17, 22, 23

[13] A. L. Hodgkin and A. F. Huxley, "The components of membrane conductance in the giant axon of loligo," *The Journal of Physiology*, vol. 116, no. 4, pp. 473–496, 1952. 2, 4

[14] A. L. Hodgkin and A. F. Huxley, "A quantitative description of membrane current and its application to conduction and excitation in nerve," *J. Physiol.*, vol. 117, pp. 500–544, 1952. 2

[15] B. Graham and D. Willshaw, "Capacity and information efficiency of the associative net," *Network: Computation in Neural Systems*, vol. 8, no. 1, p. 35, 1997. 2

[16] D. Kimura and Y. Hayakawa, "Reinforcement learning of recurrent neural network for temporal coding," *Neurocomputing*, vol. 71, no. 16-18, pp. 3379–3386, 2008. 2

[17] L. Yuan and J. G. Harris, "A spiking recurrent neural network," in *IEEE Computer Society Annual Symposium on VLSI*, pp. 321–322, 2004. 2

[18] E. M. Izhikevich, "Which model to use for cortical spiking neurons?," *IEEE transactions on neural networks*, vol. 15, no. 5, pp. 1063–1070, 2004. 3

[19] E. M. Izhikevich, "Simple model of spiking neurons," *IEEE Transactions on Neural Networks*, vol. 14, no. 6, p. 1569 – 1572, 2003. 3, 5, 21

[20] A. G. Giannari and A. Astolfi, "Model design for networks of heterogeneous hodgkin–huxley neurons," *Neurocomputing*, vol. 496, pp. 147–157, 2022. 3, 7, 8

[21] A. G. Giannari and A. Astolfi, "Model of lateral inhibition using a network of heterogeneous hodgkin- huxley neurons," in *2022 European Control Conference (ECC)*, pp. 1–6, 2022. 3, 8

[22] J. J. Letzkus, S. B. Wolff, and A. Lüthi, "Disinhibition, a circuit mechanism for associative learning and memory," *Neuron*, vol. 88, no. 2, pp. 264–276, 2015. 3

[23] D. A. McCormick, "Membrane potential and action potential," in *From Molecules to Networks (Third Edition)* (J. H.Byrne, R. Heidelberger, and i. M.Neal Waxham, eds.), pp. 351–376, Boston: Academic Press, third edition ed., 2014. 5

[24] B. W. Connors and M. J. Gutnick, "Intrinsic firing patterns of diverse neocortical neurons," *Trends in Neurosciences*, vol. 13, no. 3, pp. 99–104, 1990. 5

[25] D. M. Fox, H. G. Rotstein, and F. Nadim, *Bursting in Neurons and Small Networks*, pp. 582–596. New York, NY: Springer New York, 2022. 5

[26] R. Wilbers, A. A. Galakhova, S. L. Driessens, T. S. Heistek, V. D. Metodieva, J. Hagemann, D. B. Heyer, E. J. Mertens, S. Deng, S. Idema, *et al.*, "Structural and functional specializations of human fast-spiking neurons support fast cortical signaling," *Science advances*, vol. 9, no. 41, p. eadf0708, 2023. 5

[27] G. E. Ha and E. Cheong, "Spike frequency adaptation in neurons of the central nervous system," *Experimental neurobiology*, vol. 26, no. 4, p. 179, 2017. 5

[28] C. Ganguly, S. S. Bezugam, E. Abs, M. Payvand, S. Dey, and M. Suri, "Spike frequency adaptation: bridging neural models and neuromorphic applications," *Communications Engineering*, vol. 3, no. 1, p. 22, 2024. 5

[29] M. Pospischil, M. Toledo-Rodriguez, C. Monier, Z. Piwkowska, T. Bal, Y. Frégnac, H. Markram, and A. Destexhe, "Minimal hodgkin-huxley type models for different classes of cortical and thalamic neurons," *Biol Cybern.*, vol. 99, no. 4-5, pp. 427–441, 2008. 5

[30] A. E. Pereda, "Electrical synapses and their functional interactions with chemical synapses," *Nature Reviews Neuroscience*, vol. 15, no. 4, pp. 250–263, 2014. 7

[31] A. Destexhe, Z. F. Mainen, and T. J. Sejnowski, "An efficient method for computing synaptic conductances based on a kinetic model of receptor binding," *Neural Computation*, vol. 6, no. 1, pp. 14–18, 1994. 7, 8

[32] Y. Hao, Y. Gong, L. Wang, X. Ma, and C. Yang, "Single or multiple synchronization transitions in scale-free neuronal networks with electrical or chemical coupling," *Chaos, Solitons & Fractals*, vol. 44, no. 4-5, pp. 260–268, 2011. 7, 8

[33] D. Hebb, *The organisation of behaviour*. Wiley, New York, 1949. 9

[34] D. J. Amit, H. Gutfreund, and H. Sompolinsky, "Storing infinite numbers of patterns in a spin-glass model of neural networks," *Physical Review Letters*, vol. 55, pp. 1530–1533, Sept. 1985. 10

[35] D. J. Amit, H. Gutfreund, and H. Sompolinsky, "Spin-glass models of neural networks," *Physical Review A*, vol. 32, pp. 1007–1018, Aug. 1985. 10

[36] D. Willshaw, O. Buneman, and H. Longuet-Higgins, "Non-holographic associative memory," *Nature*, vol. 222, no. 5197, pp. 960–962, 1969. 10

[37] E. W. Weisstein, "Heaviside step function," *https://mathworld. wolfram. com/*, 2002. 10

[38] E. Gardner, "The space of interactions in neural network models," *Journal of Physics A: Mathematical and General*, vol. 21, no. 1, p. 257, 1988. 11, 19

[39] L. Topolnik and S. Tamboli, "The role of inhibitory circuits in hippocampal memory processing," *Nature Reviews Neuroscience*, vol. 23, no. 8, pp. 476–492, 2022. 14

[40] K. Kullander and L. Topolnik, "Cortical disinhibitory circuits: cell types, connectivity and function," *Trends in Neurosciences*, vol. 44, no. 8, pp. 643–657, 2021. 15

[41] D. Harnack, M. Pelko, A. Chaillet, Y. Chitour, and M. C. van Rossum, "Stability of neuronal networks with homeostatic regulation," *PLoS computational biology*, vol. 11, no. 7, p. e1004357, 2015. 16

[42] N. Sukenik, O. Vinogradov, E. Weinreb, M. Segal, A. Levina, and E. Moses, "Neuronal circuits overcome imbalance in excitation and inhibition by adjusting connection numbers," *Proceedings of the National Academy of Sciences*, vol. 118, no. 12, p. e2018459118, 2021. 16

[43] C. J. Perez Vicente and D. J. Amit, "Optimised network for sparsely coded patterns," *Journal of Physics A: Mathematical and General*, vol. 22, no. 5, pp. 559–569, 1989. 19

[44] T. Aoyagi and M. Nomura, "Oscillator neural network retrieving sparsely coded phase patterns," *Physical Review Letters*, vol. 83, pp. 1062–1065, Aug. 1999. 19

[45] C. Teeter, R. Iyer, V. Menon, N. Gouwens, D. Feng, J. Berg, A. Szafer, N. Cain, H. Zeng, M. Hawrylycz, *et al.*, "Generalized leaky integrate-and-fire models classify multiple neuron types," *Nature communications*, vol. 9, no. 1, p. 709, 2018. 21

[46] R. Brette and W. Gerstner, "Adaptive exponential integrate-and-fire model as an effective description of neuronal activity," *Journal of neurophysiology*, vol. 94, no. 5, pp. 3637–3642, 2005. 22

[47] H. Lecar, "Morris-lecar model," *Scholarpedia*, vol. 2, no. 10, p. 1333, 2007. 22

[48] M. Stimberg, R. Brette, and D. F. M. Goodman, "Brian 2, an intuitive and efficient neural simulator," *eLife*, vol. 8, p. e47314, 2019. 22

[49] Z.-q. K. Tian and D. Zhou, "Exponential time differencing algorithm for pulse-coupled hodgkin-huxley neural networks," *Frontiers in Computational Neuroscience*, vol. 14, p. 40, 2020. 23